Geophysical Research Letters

RESEARCH LETTER
10.1029/2022GL102262

The Sensitivity of Moisture Flux Partitioning in the Cold-Point Tropopause to External Forcing

C. A. Kroll[1,2], S. Fueglistaler[3], H. Schmidt[1], L. Kornblueh[1], and C. Timmreck[1]

[1]Max Planck Institute for Meteorology, Hamburg, Germany, [2]International Max Planck Research School on Earth System Modelling (IMPRS-ESM), Hamburg, Germany, [3]Program in Atmospheric and Oceanic Sciences, Princeton University, Princeton, NJ, USA

Key Points:

- Water vapor dominates the stratospheric moisture budget with a contribution of around 80% in global storm-resolving simulations
- The partitioning of stratospheric moisture fluxes into vapor and frozen hydrometeors remains stable under large temperature perturbations

Correspondence to:

C. A. Kroll,
clarissa.kroll@mpimet.mpg.de

Citation:

Kroll, C. A., Fueglistaler, S., Schmidt, H., Kornblueh, L., & Timmreck, C. (2023). The sensitivity of moisture flux partitioning in the cold-point tropopause to external forcing. *Geophysical Research Letters*, *50*, e2022GL102262. https://doi.org/10.1029/2022GL102262

Received 23 NOV 2022
Accepted 24 MAY 2023

Abstract The dryness of the stratosphere is the result of air entering through the cold tropical tropopause layer (TTL). However, our understanding of the moisture flux partitioning into water vapor and frozen hydrometeors is incomplete. This raises concerns regarding the ability of General Circulation Models to accurately predict changes in stratospheric water vapor following perturbations in the radiative budget due to volcanic aerosol or stratospheric geoengineering. We present the first results using a global storm-resolving model investigating the sensitivity of moisture fluxes within the TTL to an additional heating source. We address the question how the partitioning of moisture fluxes into water vapor and frozen hydrometeors changes under perturbations. The analysis reveals the resilience of the TTL, keeping the flux partitioning constant even at an average cold-point warming exceeding 8 K. In the control and perturbed simulations, water vapor contributes around 80% of the moisture entering the stratosphere.

Plain Language Summary The stratosphere is a dry region since moisture entering it from below has to pass the cold-point, a temperature minimum between troposphere and stratosphere. The low temperatures lead to ice formation and sedimentation of moisture. Frozen moisture within clouds rising above the cold-point tropopause can pass this temperature barrier and be injected into the stratosphere, where temperatures increase again, promoting the melting and sublimation of ice crystals. However, little is known about the sensitivity of the split of moisture entering the stratosphere into frozen and non-frozen moisture, especially under external influences, like heating by volcanic aerosol or stratospheric geoengineering efforts. Convective parameterizations in conventional simulations can lead to biases. The emerging km-scale simulations, which explicitly resolve the physical processes, offer the unique possibility to study moisture fluxes under external forcing while circumventing the downsides of parameterizations. Here, the sensitivity of the moisture flux partitioning into non-frozen and frozen components to an additional heating source is studied for the first time in global storm-resolving simulations. The analysis reveals an unaltered flux partitioning even at an average cold-point warming exceeding 8 K. In the control and perturbed simulations, water vapor contributes around 80% of the moisture entering the stratosphere.

1. Introduction

Stratospheric water vapor is important both as greenhouse gas (Forster & Shine, 2002; Solomon et al., 2010) as well as a reactant in stratospheric ozone chemistry (Ko et al., 2013). Volcanic eruptions or geoengineering interventions using sulfate aerosol perturb the stratospheric moisture budget. Pathways include the direct injection of moisture from within the volcanic plume (Joshi & Jones, 2009; Khaykin et al., 2022; Sioris et al., 2016) or aerosol-heating induced temperature changes impacting the moisture fluxes (C. Kroll, 2023; Joshi & Shine, 2003; Löffler et al., 2016). The model intercomparison projects for volcanoes and geoengineering, VolMIP (Zanchettin et al., 2016) and GeoMIP (Kravitz et al., 2015), both rely on General Circulation Model (GCM) simulations. It is unclear how reliable their moisture budgets in the stratosphere are, particularly with respect to the frozen moisture content as they only have a parameterized implementation of deep convection (Vergara-Temprado et al., 2020). Consequently, the partitioning of moisture fluxes into water vapor and frozen hydrometeors and possible changes in the partitioning under corresponding perturbations are unclear. In this study we analyze how the phase partitioning of moisture fluxes into the stratosphere is changed due to a strong heating perturbation of the tropical tropopause layer (TTL), the transition layer between radiative-convective-dynamically controlled troposphere and radiative-dynamically controlled stratosphere (Fueglistaler et al., 2009).

The stratosphere is extremely dry because virtually all moisture entering it from below has to pass the tropical cold-point tropopause. This temperature minimum between the troposphere and stratosphere causes freeze drying of air on its upwards journey, restricting the vapor content entering the stratosphere (Brewer, 1949). The correlation between specific humidity entering the stratosphere and cold-point temperatures is also evident in the well known "atmospheric tape recorder" signal (Mote et al., 1996) formed by alternating bands of lower and higher specific humidity which are dictated by seasonal variations of the cold-point temperature. This correlation of cold-point temperature and specific humidity, however, does not give information on the partitioning of moisture fluxes into large-scale upwelling water vapor and small-scale processes such as convection overshooting the cold-point tropopause, in-cloud upwelling, and turbulent mixing. This adds uncertainty to estimates of the stratospheric water vapor budget as these small-scale processes have been recognized as a non negligible source of moisture (i.e., Fueglistaler et al., 2013; Dessler et al., 2016). Efforts to quantify the contribution of frozen hydrometeors often rely on an indirect quantification of the contribution of frozen moisture with the help of trajectory models. Corresponding estimates for the frozen contribution to the moisture flux can have a low bias if coarse scale wind fields are used. Reported values include Schoeberl et al. (2018) with 2% (between 18 and −30 km), Ueyama et al. (2015) with 14% (at 100 hPa), Ueyama et al. (2018) with 15% (at 100 hPa) and Smith et al. (2022) with 26–32% (entry above 18.6 km).

The large spread of estimates demonstrates the difficulties in representing small-scale processes, especially in GCM model simulations. The situation is complicated by the fact that the convective parameterizations used in the current generation of GCMs do not reproduce all essential features of convection (i.e., Arakawa, 2004; Jones & Randall, 2011; Sherwood et al., 2014). For a description of the stratospheric water vapor budget an accurate representation of thin cirrus clouds and convection overshooting the cold-point tropopause is essential, however. Additionally some shortcomings of parametrization schemes are not immediately apparent as errors in process representation often compensate for each other (Hardiman et al., 2015).

Since computational resources are becoming more readily available and storm-resolving simulations are emerging, this problem can finally be alleviated by employing high resolution simulations which do not depend on convective parametrizations (i.e., Stevens et al., 2020). Several mesoscale studies confirm the hydration by overshooting convection (Behera et al., 2022; Chaboureau et al., 2007; Dauhut et al., 2018). Based on the analysis of a single storm Dauhut et al. (2015) estimate a frozen moisture contribution of 18%. Dauhut and Hohenegger (2022) report a frozen moisture contribution of 11%, which is the only estimate based on direct quantification using a global storm-resolving simulation. Additionally, Bolot and Fueglistaler (2021) presented the first global estimate based on observational data with a frozen contribution of around 18%.

Apart from unperturbed scenarios, the explicitly resolved deep convection overshooting the cold-point tropopause offers the possibility to predict the sensitivity of the TTL moisture fluxes to external forcing more reliably. The TTL sensitivity will be of special interest in a future where the TTL is affected by climate change and the potential employment of solar radiation management methods relying on sulfate aerosol in the lower stratosphere. We use this unprecedented opportunity and investigate the question how the moisture flux partitioning changes under perturbation. To address the question we set up a simulation pair consisting of a control (CTL) and perturbed simulation (PTB) in which the TTL is disturbed by introduction of a large heating source. This simulation pair allows us to address the question how the moisture fluxes into the stratosphere are partitioned between water vapor and frozen hydrometeors within one single framework. Additionally, the sensitivity experiment will shed light into changes of the flux partitioning at the cold-point tropopause under external perturbation. In order to get a clear signal we deliberately choose a strong forcing even if it may not be encountered in nature in this form.

In the following Section 2 the model experiments and the analysis methods are described. Section 3 summarizes the results of the study: first a quantification of the perturbation, followed by a description of the dependence of the water vapor content on the large-scale temperature field, and a discussion of the flux partitioning under perturbations. The results are discussed in Section 4.

2. Methods

2.1. Model Simulations

2.1.1. Model Setup

We use the atmosphere model of the Icosahedral Nonhydrostatic Weather and Climate Model (ICON) (Crueger et al., 2018; Giorgetta et al., 2018) and an approximately isotropic horizontal grid of 10 km. At this resolution

the model can explicitly resolve deep convection and no convective parametrization is employed (Hohenegger et al., 2020; Vergara-Temprado et al., 2020). The model encompasses 90 vertical levels up to the model top at 75 km. The sponge layer reaches down to 44 km with continuously decreasing impact. We use the sapphire physics setup (Hohenegger et al., 2022) with the PSrad radiation parametrization (Pincus & Stevens, 2013) and the one moment "three category ice scheme" (an updated version of Baldauf et al., 2011), which considers six water categories: water vapor, cloud water, rain, cloud ice, graupel and snow.

2.1.2. Experiments

Two experiments are investigated: an unperturbed run (CTL) and a run perturbed by the introduction of an additional heating source in the TTL and stratosphere up to a height of 30 km (PTB). In PTB the SSTs are fixed to those of the control run. Both CTL and PTB are run with all boundary conditions fixed to conditions for 1 January 2020. In PTB the additional heating source is realized by adding sulfate aerosol represented by monthly means of height and latitude dependent optical properties for all radiation bands of the model. The corresponding forcing fields were generated offline with the Easy Volcanic Aerosol (EVA) forcing generator (Toohey et al., 2016). EVA simulations were performed for an hypothetical equatorial volcanic eruption with a stratospheric emission of 20 Tg S. This corresponds to twice the sulfur amount emitted by the Mt. Pinatubo eruption. With the objective to generate a large tropopause perturbation the month with the highest near infrared extinction was selected and set constant throughout the simulations. The peak of the Gaussian shaped extinction profile is located at a height of 21.5 km, latitudinally the forcing is centered around the equator. Extinction values in the [20,20]°N region are relatively homogeneous, but decline rapidly toward the poles. Our analysis is based on a 60 days average after 150 days of spin-up both for CTL and PTB each.

2.2. Budget Calculations

In order to investigate the different contributions to the moisture fluxes in the TTL a budget analysis is performed. The changes in specific moisture content q_i with $i \in \{\text{frozen, non-frozen}\}$ are described by the continuity equation

$$\frac{\partial \rho q_i}{\partial t} = \left(\frac{\partial \rho q_i u}{\partial x} + \frac{\partial \rho q_i v}{\partial y} + \frac{\partial \rho q_i w}{\partial z}\right) - \left(\frac{\partial \rho q_i w_{sedi,i}}{\partial z}\right) + \nabla(D \nabla \rho q_i) + \sigma_i, \quad (1)$$

where the first three terms on the right hand side of the equation describe the advective transport of the specific moisture q_i through the atmosphere of density ρ with the velocities u, v or w, the fourth term the flux due to the sedimentation velocity $w_{sedi,i}$, the fifth term the parameterized component of turbulent mixing with diffusion constant D, and σ_i accounts for the sources and sinks of moisture due to microphysical conversion processes between frozen and non-frozen phases. For our budget calculations we use the vertical flux terms due to advection, sedimentation and turbulent mixing.

Special care is taken to ensure mass conservation within the analysis. We circumvent issues arising from the mixing of variables calculated in different subsequent calculation steps, by adding advection and sedimentation fluxes, as well as the microphysical tendencies, as output streams to ICON allowing for a direct online calculation. The quality of our analysis also depends on the handling of the Courant-Friedrichs-Lewy criterion (CFL, Courant et al., 1928) and the choice of model surface on which the analysis is performed. Violations of the CFL criterion are prevented in the model by velocity damping. This damping, however, may create or delete tracer mass in extreme cases. To prevent this the time step is reduced to a quarter of the default time step for the used resolution. This reduces the distance which can be traveled by air parcels within one time step and thus the probability to pass through multiple grid cells within one integration step. All calculations are performed on the native grid to ensure a closed budget.

2.3. Choice of Reference Height

The moisture budget calculation is carried out on the original native grid. For the calculation of the moisture flux the time and spatial average of the total fluxes in the area between [−30,30]°N is computed and then evaluated at the height level nearest to the correspondingly averaged cold-point tropopause height. The latter is defined here as the lowest temperature between troposphere and stratosphere on height levels of around 500–700 m spacing in the TTL. Any reference to the tropopause in the text hereafter consequently refers to the average cold-point

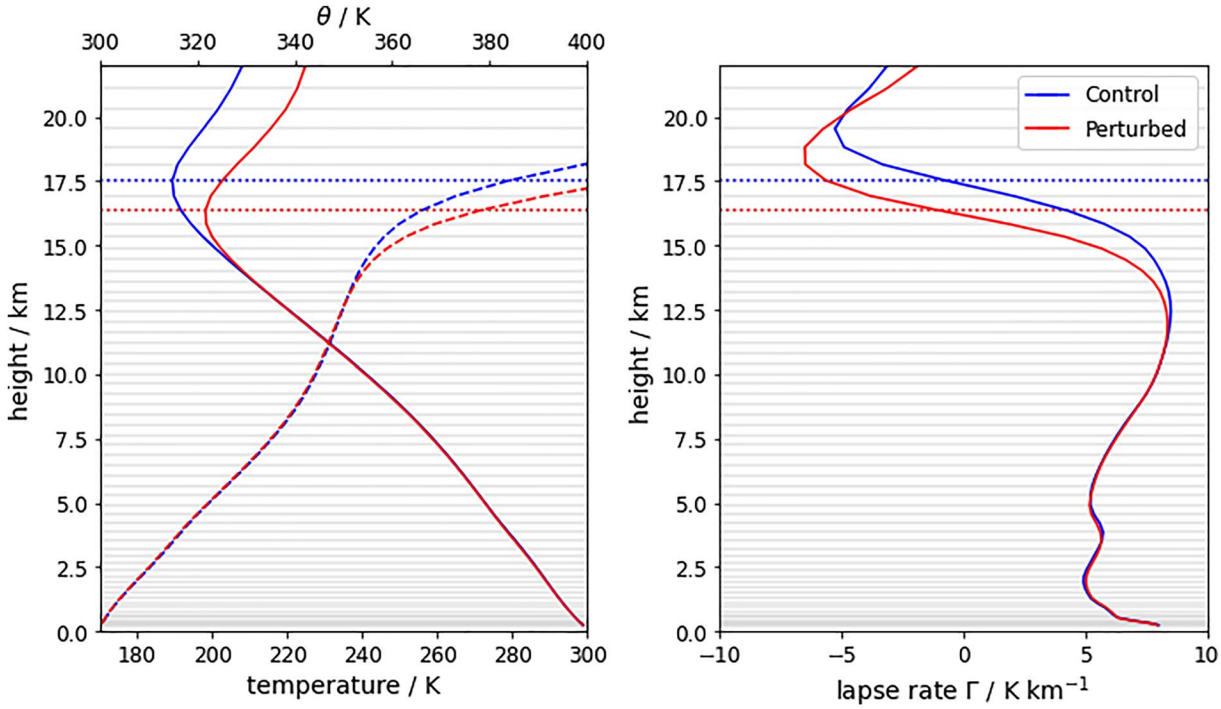

Figure 1. Left panel: temperature (solid line) and potential temperature profile (θ, dashed line). Right panel: lapse rate profile for temperature. An average over the inner tropical region between [−5,5]°N is taken for both plots. Control is shown in blue, Perturbed in red. The dotted line indicates the height of the cold-point tropopause. The gray lines indicate the height levels.

tropopause. Although this vertical resolution will not allow for a replication of radio-sounding measurements (Gettelman & Forster, 2002), we chose it as Dauhut and Hohenegger (2022) showed that it is possible to compute a moisture budget at this grid spacing.

3. Results

3.1. Quantifying the Perturbation

Figure 1 shows the inner tropical (potential) temperature and lapse rate profiles of the Control (CTL, blue) and Perturbed (PTB, red) simulations. The heating starts to take effect at a height of around 12.5 km, but is most prominent in the TTL and lower stratosphere. Table 1 summarizes the changes in the physical parameters of CTL and PTB relevant for this study: The cold-point tropopause height is shifted downwards by (1.1 ± 0.6) km. The corresponding uncertainty in the cold-point height is the upper limit for the error made if the average cold-point were located one model level lower or higher than calculated. The mean and lowest 10th percentile of cold-point tropopause temperature rise by 8.9 and 9.2 K, respectively. The increases in saturation specific humidity caused by the elevated cold-point temperatures enhance the specific humidity values at the cold-point by more than 200%. To put these values in context, both the changes in cold-point temperature and specific humidity are between three and four times larger than the amplitudes of their seasonal variations at the cold-point tropopause (i.e., Seidel et al., 2001).

Table 1
Two-Monthly Average [−5,5]°N Tropical Cold-Point Tropopause Height, Temperature, 10th Percentile Temperature and Specific Humidity in the Control and Perturbed Simulations

	CTL	PTB	Δ (PTB − CTL)
Tropopause height (km)	17.5	16.4	−1.1
Tropopause temperature (K)	189.3	198.2	+8.9
10th percentile of tropopause temperature (K)	186.8	195.9	+9.2
Tropopause water vapor (ppmv)	2.1	6.7	+4.6 (+219%)

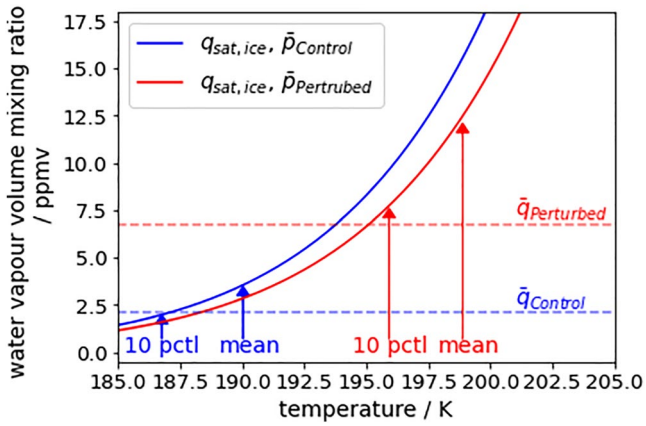

Figure 2. Two-months average water vapor mixing ratio at the mean cold-point height for CTL (blue) and PTB (red) in the inner tropics between [−5,5]°N, marked by horizontal dashed lines. The average water vapor values are compared against the expected saturation water vapor mixing ratio at the mean cold-point temperature and the 10th percentile of cold-point temperatures for CTL and PTB, marked with arrows. The solid curves mark the saturation mixing ratio above ice as function of temperature at the cold-point pressure as implemented in ICON (COSMO, Doms et al., 2021) for CTL and PTB.

3.2. Water Vapor Distribution at the Cold-Point Tropopause

Figure 2 visualizes the average water vapor at the cold-point for CTL (blue) and PTB (red) in relation to the temperature dependent saturation water vapor mixing ratio as implemented in ICON (Doms et al., 2021). In PTB the average water vapor is about three times higher than in CTL due to the cold-point warming. Nevertheless, the large-scale picture of the dependence of the average water vapor on the cold-point temperature remains unchanged. In line with previous studies, the model results show that the vapor at the cold point scales well with an equivalent frost point temperature. The water vapor at the cold point is dictated by the lowest temperatures in the inner tropics (Fueglistaler & Haynes, 2005; Oman et al., 2008). Here the 10th percentile of cold-point temperatures in the [−5,5]°N region describes the vapor values for CTL and PTB. For PTB, the estimate using the 10th percentile of cold-point temperatures slightly exceeds (+10%) the model's water vapor mixing ratio. This discrepancy may be explained by an increase in the horizontal velocities at the cold-point tropopause (+14%) and enhanced variability of the cold-point temperatures (±4%). Nevertheless, the correlation between saturation water vapor mixing ratio and the 10th percentile of cold-point temperatures remains a good indicator to estimate the average water vapor at the cold-point, also for the perturbed case. It is only shifted according to the 9 K ΔT of cold-point warming (compare Table 1). The 10th percentile of cold-point temperatures in Control and Perturbed can consequently be seen as the equivalent frost point temperature of the TTL in this simulation.

3.3. Change in Flux Partitioning

Figure 3 shows the contribution from water vapor and frozen hydrometeors to the total flux for CTL (blue) and PTB (red) (The plot shows unrounded values, the calculated percentage changes therefore deviate slightly from those calculated based on the values reported in the text.). A first inspection of the CTL data reveals that the frozen moisture flux of 0.0006 kg m^{-2} $year^{-1}$ contributes with around 20%, a value which is well within the spread of values reported in previous studies (e.g., Dauhut et al., 2015; Dauhut & Hohenegger, 2022; Schoeberl et al., 2018; Smith et al., 2022; Ueyama et al., 2015, 2018). The leading order term however is the water vapor flux of 0.0021 kg m^{-2} $year^{-1}$ contributing around 80% to the total flux. The computed water vapor values and water vapor fluxes at the cold point are also consistent with observations in January (Fueglistaler et al., 2009; Sioris et al., 2016). In PTB the water vapor flux is enhanced to 0.0081 kg m^{-2} $year^{-1}$ by a factor of four. However, the flux of frozen hydrometeors is increased

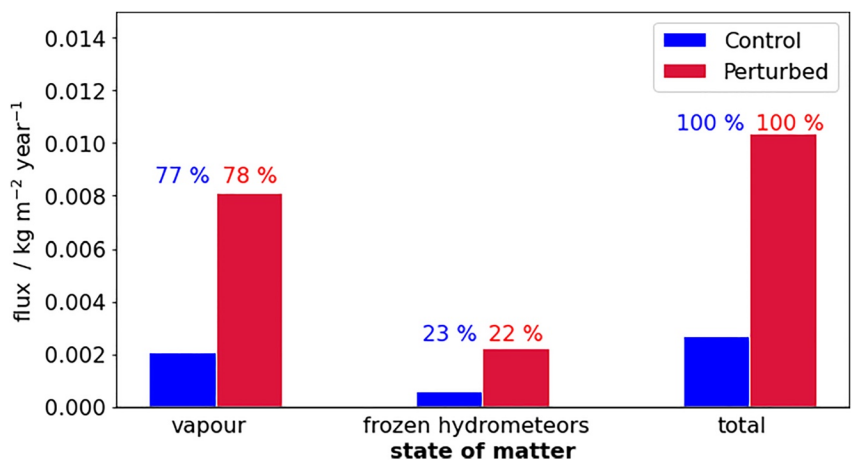

Figure 3. Two-month average of the moisture fluxes at the average cold-point tropopause in the region between [−30,30]°N. The contribution of water vapor and frozen hydrometeors is shown along with the total. The control simulation is shown in blue, the perturbed simulations in red. Above the bars the corresponding share of the total moisture flux is shown.

by almost the same factor to 0.0023 kg m^{-2} $year^{-1}$. This means that the partitioning into fluxes of water vapor and frozen hydrometeors remains virtually unchanged despite the strong perturbation of the TTL in the PTB experiment.

4. Discussion

We used ICON, a strom-resolving global model, to study the sensitivity of the moisture flux partitioning in the TTL to external forcing. The base simulation is in line with previously published data on moisture flux partitioning in non-frozen and frozen contributions. Our 20% contribution is in agreement with the 18% frozen contribution found in the observational based study by Bolot and Fueglistaler (2021). ICON was used by Dauhut and Hohenegger (2022) as well, their estimates are 11%, when only considering the deepest convection, and 29%, when considering all hydrometeors. The calculations are not directly comparable, though, for three reasons. First, they rely on a higher horizontal resolution and a slightly different physics package. Second, their analysis is based on tendencies calculated offline. Third, they indirectly inferred the frozen moisture contribution, rather than directly calculating fluxes online as in our study. Our result also falls into the range of 2%–32% frozen moisture contribution reported in GCM studies (Schoeberl et al., 2018; Smith et al., 2022; Ueyama et al., 2015, 2018).

The analysis shows that in response to the strong tropopause perturbation, the moisture flux partitioning remains almost constant—even for a very strong perturbation with an average increase of cold-point temperatures by over 8 K. The constant share of frozen moisture to the total moisture entering the stratosphere underlines the character of the TTL as a layer which is set by a balance between radiative-dynamically induced temperature changes in the stratosphere and temperature changes due to convective-radiative-dynamical process from the troposphere (Fueglistaler et al., 2009).

The result of roughly constant partitioning may surprise at first, but is consistent with a trajectory model based climate change study (Smith et al., 2022), where ice content was explicitly tracked. Observational based studies analyzing the annual cycle (Fueglistaler et al., 2013; Liu et al., 2010) also found a constant frozen hydrometeor contribution, which can calculated from the offset between observed and modeled water vapor values. Here the frozen moisture flux is calculated directly. The agreement on the constant partitioning despite the different analysis method indicates that the robustness of the moisture flux partitioning in the TTL is not exclusive to a perturbation in form of an heating layer, as in our volcanic or geoengineering scenarios, but has also holds for other disturbances such as seasonal variations and climate change.

The constant partitioning of moisture fluxes into frozen and non-frozen states of matter demonstrates that the large-scale temperature field determines both moisture fluxes entering the stratosphere for these various perturbations. Frozen and non-frozen moisture follows the Clausius Clapeyron scaling. Consequently, the total flux can be thought of as a water vapor flux controlled by an equivalent frost point temperature, whereas the flux of frozen hydrometeors is given by an additional constant temperature offset ΔT. Based on a 12% increase of specific humidity per Kelvin in the cold-point region (C. A. Kroll et al., 2021), this offset gives an estimate of the constant relative contribution of frozen moisture to the total budget.

The contribution of frozen moisture to the total stratospheric moisture budget is still largely uncertain, especially in the current generation of GCMs. The agreement on the constant partitioning between our direct quantification in a storm-resolving framework and the indirect quantification in a framework relying on convective parametrization in a GCM (Smith et al., 2022) is therefore encouraging.

In summary, the result of the analysis shows that the moisture flux partitioning at the cold-point tropopause is robust, even under large perturbations. The explicitly resolved deep convection in our numerical model increases the confidence that this result is not a model artifact. The actual numbers presented in this study may be model specific and sensitive to the choice of microphysical parametrization (Hu et al., 2021; Lamraoui et al., 2023; van Zanten et al., 2011). Further constraints of the contribution of frozen moisture to the total flux based on observations are needed and may be complemented by simulations with even higher resolution.

Data Availability Statement

The ICON model is available to individuals (https://mpimet.mpg.de/en/research/modeling). Simulations were carried out with the code version in branch icon-aes-CaVE-test005. All data shown in the figures and scripts needed to generate the figures in this work are available from the MPI publication repository under https://hdl.handle.net/21.11116/0000-000B-5D17-4.

Acknowledgments
We thank Blaž Gasparini and two anonymous reviewers for their comments and suggestions. This research has been supported by the Deutsche Forschungsgemeinschaft (DFG) Research Unit VolImpact (FOR2820, Grant: 398006378) within the projects VolDyn and VolClim. CK is a member of the International Max Planck Research School (IMPRS). Her research stay at Princeton was supported by the Fueglistaler group. HS acknowledges support from the SOCTOC project of the BMBF research initiative ROMIC2. The data was processed using CDO (https://code.mpimet.mpg.de/projects/cdo/embedded/cdo.pdf) and the resources at the Deutsche Klimarechenzentrum (DKRZ) granted by its Scientific Steering Committee (WLA) under project ID bb1093. For parts of the analysis the open source libraries "easyd" by M. Roßmy (https://github.com/matti-82/easyd) and "netcdfd" by J. Colvin (https://code.dlang.org/packages/netcdf) were employed. We thank H. Franke, A. Schneidereit, U. Niemeier, J. Bao, and L. Kluft for discussing different aspects of this work with the authors. Open access funding enabled and organized by Projekt DEAL.

References

Arakawa, A. (2004). The cumulus parameterization problem: Past, present, and future. *Journal of Climate*, *17*(13), 2493–2525. https://doi.org/10.1175/1520-0442(2004)017<2493:ratcpp>2.0.co;2

Baldauf, M., Seifert, A., Förstner, J., Majewski, D., Raschendorfer, M., & Reinhardt, T. (2011). Operational convective-scale numerical weather prediction with the COSMO model: Description and sensitivities. *Monthly Weather Review*, *139*(12), 3887–3905. https://doi.org/10.1175/MWR-D-10-05013.1

Behera, A. K., Rivière, E. D., Khaykin, S. M., Marécal, V., Ghysels, M., Burgalat, J., & Held, G. (2022). On the cross-tropopause transport of water by tropical convective overshoots: A mesoscale modelling study constrained by in situ observations during the TRO-Pico field campaign in Brazil. *Atmospheric Chemistry and Physics*, *22*(2), 881–901. https://doi.org/10.5194/acp-22-881-2022

Bolot, M., & Fueglistaler, S. (2021). Tropical water fluxes dominated by deep convection up to near tropopause levels. *Geophysical Research Letters*, *48*(4), e2020GL091471. https://doi.org/10.1029/2020GL091471

Brewer, A. W. (1949). Evidence for a world circulation provided by the measurements of helium and water vapour distribution in the stratosphere. *Quarterly Journal of the Royal Meteorological Society*, *75*(326), 351–363. https://doi.org/10.1002/qj.49707532603

Chaboureau, J.-P., Cammas, J.-P., Duron, J., Mascart, P. J., Sitnikov, N. M., & Voessing, H.-J. (2007). A numerical study of tropical cross-tropopause transport by convective overshoots. *Atmospheric Chemistry and Physics*, *7*(7), 1731–1740. https://doi.org/10.5194/acp-7-1731-2007

Courant, R., Friedrichs, K., & Lewy, H. (1928). Über die partiellen Differenzengleichungen der mathematischen Physik. *Mathematische Annalen*, *100*(1), 32–74. https://doi.org/10.1007/BF01448839

Crueger, T., Giorgetta, M. A., Brokopf, R., Esch, M., Fiedler, S., Hohenegger, C., et al. (2018). ICON-A, the atmosphere component of the ICON earth system model: II. Model evaluation. *Journal of Advances in Modeling Earth Systems*, *10*(7), 1638–1662. https://doi.org/10.1029/2017MS001233

Dauhut, T., Chaboureau, J.-P., Escobar, J., & Mascart, P. (2015). Large-eddy simulations of Hector the convector making the stratosphere wetter. *Atmospheric Science Letters*, *16*(2), 135–140. https://doi.org/10.1002/asl2.534

Dauhut, T., Chaboureau, J.-P., Haynes, P. H., & Lane, T. P. (2018). The mechanisms leading to a stratospheric hydration by overshooting convection. *Journal of the Atmospheric Sciences*, *75*(12), 4383–4398. https://doi.org/10.1175/JAS-D-18-0176.1

Dauhut, T., & Hohenegger, C. (2022). The contribution of convection to the stratospheric water vapor: The first budget using a global storm-resolving model. *Journal of Geophysical Research: Atmospheres*, *127*(5), e2021JD036295. https://doi.org/10.1029/2021JD036295

Dessler, A., Ye, H., Wang, T., Schoeberl, M., Oman, L., Douglass, A., et al. (2016). Transport of ice into the stratosphere and the humidification of the stratosphere over the 21st century. *Geophysical Research Letters*, *43*(5), 2323–2329. https://doi.org/10.1002/2016GL067991

Doms, G., Förstner, J., Heise, E., Herzog, H.-J., Mironov, D., Raschendorfer, M., et al. (2021). A description of the nonhydrostatic regional COSMO-model Part II physical parameterizations (Tech. Rep. No. 333 COSMO 6.00). Deutscher Wetterdienst. Retrieved from http://www.cosmo-model.org/content/model/documentation/core/cosmo_physics_6.00.pdf

Forster, P. M. d. F., & Shine, K. P. (2002). Assessing the climate impact of trends in stratospheric water vapor. *Geophysical Research Letters*, *29*(6), 10-1–10-4. https://doi.org/10.1029/2001GL013909

Fueglistaler, S., Dessler, A. E., Dunkerton, T. J., Folkins, I., Fu, Q., & Mote, P. W. (2009). Tropical tropopause layer. *Reviews of Geophysics*, *47*(1), 1606. https://doi.org/10.1029/2008RG000267

Fueglistaler, S., & Haynes, P. H. (2005). Control of interannual and longer-term variability of stratospheric water vapor. *Journal of Geophysical Research*, *110*(D24), D24108. https://doi.org/10.1029/2005JD006019

Fueglistaler, S., Liu, Y. S., Flannaghan, T. J., Haynes, P. H., Dee, D. P., Read, W. J., et al. (2013). The relation between atmospheric humidity and temperature trends for stratospheric water. *Journal of Geophysical Research: Atmospheres*, *118*(2), 1052–1074. https://doi.org/10.1002/jgrd.50157

Gettelman, A., & Forster, P. M. d. F. (2002). A climatology of the tropical tropopause layer. *Journal of the Meteorological Society of Japan. Series II*, *80*(4B), 911–924. https://doi.org/10.2151/jmsj.80.911

Giorgetta, M. A., Brokopf, R., Crueger, T., Esch, M., Fiedler, S., Helmert, J., et al. (2018). ICON-A, the atmosphere component of the ICON earth system model: I. Model description. *Journal of Advances in Modeling Earth Systems*, *10*(7), 1613–1637. https://doi.org/10.1029/2017MS001242

Hardiman, S. C., Boutle, I. A., Bushell, A. C., Butchart, N., Cullen, M. J. P., Field, P. R., et al. (2015). Processes controlling tropical tropopause temperature and stratospheric water vapor in climate models. *Journal of Climate*, *28*(16), 6516–6535. https://doi.org/10.1175/JCLI-D-15-0075.1

Hohenegger, C., Korn, P., Linardakis, L., Redler, R., Schnur, R., Adamidis, P., et al. (2022). ICON-Sapphire: Simulating the components of the earth system and their interactions at kilometer and subkilometer scales. *Geoscientific Model Development Discussions*, *2022*, 1–42. https://doi.org/10.5194/gmd-2022-171

Hohenegger, C., Kornblueh, L., Klocke, D., Becker, T., Cioni, G., Engels, J. F., et al. (2020). Climate statistics in global simulations of the atmosphere, from 80 to 2.5 km grid spacing. *Journal of the Meteorological Society of Japan. Series II*, *98*(1), 73–91. https://doi.org/10.2151/jmsj.2020-005

Hu, Z., Lamraoui, F., & Kuang, Z. (2021). Influence of upper-troposphere stratification and cloud–radiation interaction on convective overshoots in the tropical tropopause layer. *Journal of the Atmospheric Sciences*, *78*(8), 2493–2509. https://doi.org/10.1175/JAS-D-20-0241.1

Jones, T. R., & Randall, D. A. (2011). Quantifying the limits of convective parameterizations. *Journal of Geophysical Research*, *116*(D8), D08210. https://doi.org/10.1029/2010JD014913

Joshi, M. M., & Jones, G. S. (2009). The climatic effects of the direct injection of water vapour into the stratosphere by large volcanic eruptions. *Atmospheric Chemistry and Physics*, *9*(16), 6109–6118. https://doi.org/10.5194/acp-9-6109-2009

Joshi, M. M., & Shine, K. P. (2003). A GCM study of volcanic eruptions as a cause of increased stratospheric water vapor. *Journal of Climate*, *16*(21), 3525–3534. https://doi.org/10.1175/1520-0442(2003)016<3525:AGSOVE>2.0.CO;2

Khaykin, S., Podglajen, A., Ploeger, F., Grooß, J.-U., Tence, F., Bekki, S., et al. (2022). Global perturbation of stratospheric water and aerosol burden by Hunga eruption. *Communications Earth & Environment*, *3*(1), 316. https://doi.org/10.1038/s43247-022-00652-x

Ko, M. K. W., Newman, P. A., Reimann, S., & Strahan, S. E. (2013). *SPARC report on lifetimes of stratospheric ozone-depleting substances, their replacements, and related species* (SPARC Report Volume: No. 6. Tech. Rep.). SPARC Office. Backup Publisher: SPARC. Retrieved from http://www.sparc-climate.org/publications/sparc-reports/

Kravitz, B., Robock, A., Tilmes, S., Boucher, O., English, J. M., Irvine, P. J., et al. (2015). The geoengineering model intercomparison project phase 6 (GeoMIP6): Simulation design and preliminary results. *Geoscientific Model Development*, *8*(10), 3379–3392. https://doi.org/10.5194/gmd-8-3379-2015

Kroll, C. (2023). The volcanic impact on moisture fluxes into the stratosphere (PhD thesis). University of Hamburg. Retrieved from https://pure.mpg.de/pubman/faces/ViewItemFullPage.jsp?itemId=item_3489355_3

Kroll, C. A., Dacie, S., Azoulay, A., Schmidt, H., & Timmreck, C. (2021). The impact of volcanic eruptions of different magnitude on stratospheric water vapor in the tropics. *Atmospheric Chemistry and Physics*, *21*(8), 6565–6591. https://doi.org/10.5194/acp-21-6565-2021

Lamraoui, F., Krämer, M., Afchine, A., Sokol, A. B., Khaykin, S., Pandey, A., & Kuang, Z. (2023). Sensitivity of convectively driven tropical tropopause cirrus properties to ice habits in high-resolution simulations. *Atmospheric Chemistry and Physics*, *23*(4), 2393–2419. https://doi.org/10.5194/acp-23-2393-2023

Liu, Y. S., Fueglistaler, S., & Haynes, P. H. (2010). Advection-condensation paradigm for stratospheric water vapor. *Journal of Geophysical Research*, *115*(D24), 1–18. https://doi.org/10.1029/2010JD014352

Löffler, M., Brinkop, S., & Jöckel, P. (2016). Impact of major volcanic eruptions on stratospheric water vapour. *Atmospheric Chemistry and Physics*, *16*(10), 6547–6562. https://doi.org/10.5194/acp-16-6547-2016

Mote, P. W., Rosenlof, K. H., McIntyre, M. E., Carr, E. S., Gille, J. C., Holton, J. R., et al. (1996). An atmospheric tape recorder: The imprint of tropical tropopause temperatures on stratospheric water vapor. *Journal of Geophysical Research*, *101*(D2), 3989–4006. https://doi.org/10.1029/95JD03422

Oman, L., Waugh, D. W., Pawson, S., Stolarski, R. S., & Nielsen, J. E. (2008). Understanding the changes of stratospheric water vapor in coupled chemistry climate model simulations. *Journal of the Atmospheric Sciences*, *65*(10), 3278–3291. https://doi.org/10.1175/2008JAS2696.1

Pincus, R., & Stevens, B. (2013). Paths to accuracy for radiation parameterizations in atmospheric models. *Journal of Advances in Modeling Earth Systems*, *5*(2), 225–233. https://doi.org/10.1002/jame.20027

Schoeberl, M. R., Jensen, E. J., Pfister, L., Ueyama, R., Avery, M., & Dessler, A. E. (2018). Convective hydration of the upper troposphere and lower stratosphere. *Journal of Geophysical Research: Atmospheres*, *123*(9), 4583–4593. https://doi.org/10.1029/2018JD028286

Seidel, D. J., Ross, R. J., Angell, J. K., & Reid, G. C. (2001). Climatological characteristics of the tropical tropopause as revealed by radiosondes. *Journal of Geophysical Research*, *106*(D8), 7857–7878. https://doi.org/10.1029/2000JD900837

Sherwood, S. C., Bony, S., & Dufresne, J.-L. (2014). Spread in model climate sensitivity traced to atmospheric convective mixing. *Nature*, *505*(7481), 37–42. https://doi.org/10.1038/nature12829

Sioris, C. E., Malo, A., McLinden, C. A., & D'Amours, R. (2016). Direct injection of water vapor into the stratosphere by volcanic eruptions. *Geophysical Research Letters*, *43*(14), 7694–7700. https://doi.org/10.1002/2016GL069918

Smith, J. W., Bushell, A. C., Butchart, N., Haynes, P. H., & Maycock, A. C. (2022). The effect of convective injection of ice on stratospheric water vapor in a changing climate. *Geophysical Research Letters*, *49*(9), e2021GL097386. https://doi.org/10.1029/2021GL097386

Solomon, S., Rosenlof, K. H., Portmann, R. W., Daniel, J. S., Davis, S. M., Sanford, T. J., & Plattner, G.-K. (2010). Contributions of stratospheric water vapor to decadal changes in the rate of global warming. *Science (New York, N.Y.)*, *327*(5970), 1219–1223. https://doi.org/10.1126/science.1182488

Stevens, B., Acquistapace, C., Hansen, A., Heinze, R., Klinger, C., Klocke, D., et al. (2020). The added value of large-eddy and storm-resolving models for simulating clouds and precipitation. *Journal of the Meteorological Society of Japan. Series II*, *98*(2), 395–435. https://doi.org/10.2151/jmsj.2020-021

Toohey, M., Stevens, B., Schmidt, H., & Timmreck, C. (2016). Easy volcanic aerosol (EVA v1.0): An idealized forcing generator for climate simulations. *Geoscientific Model Development*, *9*(11), 4049–4070. https://doi.org/10.5194/gmd-9-4049-2016

Ueyama, R., Jensen, E. J., & Pfister, L. (2018). Convective influence on the humidity and clouds in the tropical tropopause layer during boreal summer. *Journal of Geophysical Research: Atmospheres*, *123*(14), 7576–7593. https://doi.org/10.1029/2018JD028674

Ueyama, R., Jensen, E. J., Pfister, L., & Kim, J.-E. (2015). Dynamical, convective, and microphysical control on wintertime distributions of water vapor and clouds in the tropical tropopause layer. *Journal of Geophysical Research: Atmospheres*, *120*(19), 10483–10500. https://doi.org/10.1002/2015JD023318

van Zanten, M. C., Stevens, B., Nuijens, L., Siebesma, A. P., Ackerman, A. S., Burnet, F., et al. (2011). Controls on precipitation and cloudiness in simulations of trade-wind cumulus as observed during RICO. *Journal of Advances in Modeling Earth Systems*, *3*(2), 1–19. https://doi.org/10.1029/2011MS000056

Vergara-Temprado, J., Ban, N., Panosetti, D., Schlemmer, L., & Schär, C. (2020). Climate models permit convection at much coarser resolutions than previously considered. *Journal of Climate*, *33*(5), 1915–1933. https://doi.org/10.1175/JCLI-D-19-0286.1

Zanchettin, D., Khodri, M., Timmreck, C., Toohey, M., Schmidt, A., Gerber, E. P., et al. (2016). The model intercomparison project on the climatic response to volcanic forcing (VolMIP): Experimental design and forcing input data for CMIP6. *Geoscientific Model Development*, *9*(8), 2701–2719. https://doi.org/10.5194/gmd-9-2701-2016